Fuzzy Clock

Decision-Specific Timing Information
Online Appendix

Chae-Yeon Xon
Yonsei University

September 2026

Abstract

This appendix contains proofs and additional calculations for the paper. The two main moment-order and decision-order proofs appear with their theorems in the paper. Appendix A develops supporting additive-clock and moment identities. Appendices B–D cover clock actions, linear queries, and cohort mixing. Appendices E–G give estimated-operator, projection, and clock-set calculations. Appendix H collects numerical illustrations. Appendix I documents the gas data and timing calculations. Appendix J contains the policy and storage-option calculations.

JEL Codes: C14, C18, C21, C32, F51, Q41

Keywords: event time, event study, treatment timing, inverse problems, counterfactual identification, partial identification, natural gas

Yonsei University. Email: eunixon@yonsei.ac.kr. This draft is circulated for discussion; comments and suggestions are welcome.

Contents

Appendix A. Additive-Clock Results

A.1. Clock distortion

PROPOSITION A1 (Recorded-clock mapping). *Let $p_u = \mathbb{P}(U = u)$. For each recorded horizon ℓ,*

$$m_\ell = (A_p\tau)_\ell = \sum_{u\in\mathbb{Z}} p_u \tau_{\ell+u}. \tag{A1}$$

If $\check{p}_j = p_{-j}$, then $m = \check{p} * \tau$.

PROOF OF PROPOSITION A1. For a recorded horizon ℓ, the latent horizon equals $\ell + U$. Conditional expectation and Assumption 1 give

$$m_\ell = \sum_{u\in\mathbb{Z}} \mathbb{P}(U = u)\mathbb{E}[\tau_{i,\ell+u} \mid U = u] = \sum_{u\in\mathbb{Z}} p_u \tau_{\ell+u}. \tag{A2}$$

Set $j = -u$. Since $\check{p}_j = p_{-j}$,

$$m_\ell = \sum_{j\in\mathbb{Z}} \check{p}_j \tau_{\ell-j} = (\check{p} * \tau)_\ell. \tag{A3}$$

□

Figure A1 applies (A1) with $\mathbb{P}(U = 0) = \mathbb{P}(U = 2) = 1/2$ to a finite-support response.

A.2. Recorded leads

Suppose the latent response satisfies $\tau_h = 0$ for $h < 0$. For any recorded lead $\ell < 0$,

$$m_\ell = \sum_{u\geq-\ell} p_u \tau_{\ell+u}. \tag{A4}$$

A positive delay probability and a post-event response place causal mass in recorded leads. The sign follows the sign of the response terms entering the sum. Recorded leads can reflect clock delay, response heterogeneity, or a deviation in the untreated counterfactual trend. These channels correspond to separate restrictions.

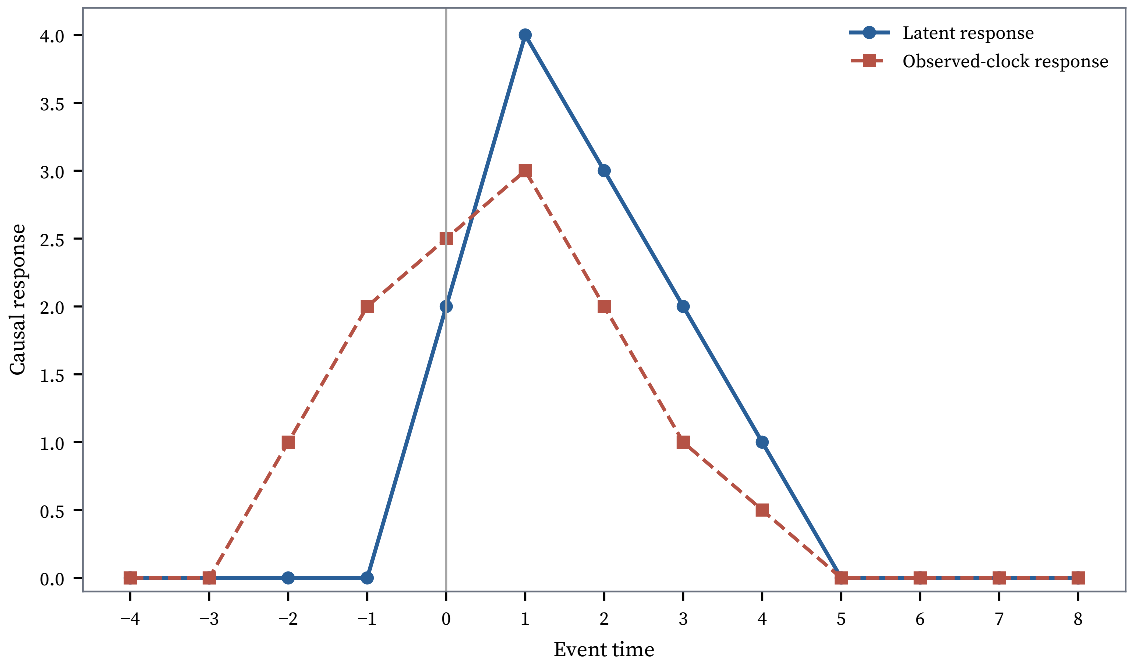

FIGURE A1. Latent and recorded-clock response paths

The latent response equals zero at negative horizons and equals 2, 4, 3, 2, 1 at horizons zero through four. The recorded clock satisfies $\mathbb{P}(U = 0) = \mathbb{P}(U = 2) = 1/2$. The recorded-clock response is $m_\ell = \{\tau_\ell + \tau_{\ell+2}\}/2$.

A.3. Finite-window accumulation

PROPOSITION A2 (Finite-window accumulation). *For integers $a \le b$, suppose $\sum_u p_u |\tau_{\ell+u}| < \infty$ for each $\ell = a, \dots, b$. Then*

$$\sum_{\ell=a}^{b} m_\ell = \sum_{h \in \mathbb{Z}} \tau_h \mathbb{P}(h - b \le U \le h - a). \tag{A5}$$

PROOF OF PROPOSITION A2. Absolute summability on the displayed finite window permits an exchange of sums:

$$\sum_{\ell=a}^{b} m_\ell = \sum_{\ell=a}^{b} \sum_u p_u \tau_{\ell+u} = \sum_u p_u \sum_{\ell=a}^{b} \tau_{\ell+u}. \tag{A6}$$

Set $h = \ell + u$. The restriction $a \le \ell \le b$ becomes $h - b \le u \le h - a$. Hence

$$\sum_{\ell=a}^{b} m_\ell = \sum_h \tau_h \sum_{u=h-b}^{h-a} p_u = \sum_h \tau_h \mathbb{P}(h - b \le U \le h - a). \tag{A7}$$

$\square$

A.4. Temporal-moment transport and moment order

The supporting moment-interchange and transport arguments are recorded here.

LEMMA A1 (Moment interchange). *If* $\sum_h(1+|h|^r)|\tau_h| < \infty$ *and* $\mathbb{E}|U|^r < \infty$*, then*

$$\sum_{\ell,u} |\ell|^r p_u |\tau_{\ell+u}| < \infty.$$

PROOF. Write $h = \ell + u$, so $|\ell|^r = |h-u|^r \le 2^{r-1}(|h|^r + |u|^r)$ for $r \ge 1$. Then

$$\sum_{\ell,u} |\ell|^r p_u |\tau_{\ell+u}| = \sum_{h,u} |h-u|^r p_u |\tau_h| \tag{A8}$$

$$\le 2^{r-1}\left\{\sum_h |h|^r|\tau_h| + \mathbb{E}|U|^r \sum_h |\tau_h|\right\} < \infty. \tag{A9}$$

The case $r = 0$ follows from $\tau \in \ell^1$. □

DETAILED PROOF OF PROPOSITION 3. For $j \le r$, reindex $T_j(S_u x)$:

$$T_j(S_u x) = \sum_h h^j x_{h+u} = \sum_z (z-u)^j x_z \tag{A10}$$

$$= \sum_{k=0}^{j} \binom{j}{k} (-u)^{j-k} T_k(x). \tag{A11}$$

These component equations give $\mathbf{T}_r(S_u x) = \Pi_r(u)\mathbf{T}_r(x)$. Lemma A1 permits averaging over U, which gives

$$\mathbf{M}_r = \mathbb{E}[\Pi_r(U)]\mathbf{T}_r. \tag{A12}$$

The r-th row equals

$$M_r = \sum_{k=0}^{r} \binom{r}{k} (-1)^k \mu_k T_{r-k}. \tag{A13}$$

The diagonal entries of $\mathbb{E}[\Pi_r(U)]$ equal one, so

$$T_r = M_r - \sum_{k=1}^{r} \binom{r}{k} (-1)^k \mu_k T_{r-k}. \tag{A14}$$

Starting from $T_0 = M_0$, the recursion determines moments through order r. □

PROOF OF COROLLARY 1. Set $r = 0$ in (25). The identity becomes $M_0 = \mu_0 T_0 = T_0$. □

PROOF OF COROLLARY 2. Set $r = 1$ and $r = 2$ in (25) and solve recursively. For the distribution statement, let H have mass $q_h = \tau_h/T_0$, let U have clock law p, and let $L = H - U$. The recorded causal-mass distribution is the law of L. Under the product law $q \times p$, $\mathbb{E}H = \mathbb{E}L + \mathbb{E}U$ and $\mathrm{Var}(H) = \mathrm{Var}(L) - \mathrm{Var}(U)$. □

A.5. Response-dependent recording: location of the identities

The query cross-moment identity yields the first- and second-order covariance corrections. A two-cell construction shows how a pooled marginal clock differs from cell-specific mixing.

Appendix B. Clock-Action Results

B.1. Pathwise queries and translation

The temporal-moment results concern population averages. For a realized path, query recovery follows the action of one displacement. Orbit notation collects the latent paths compatible with a recorded path and displacement support. First-passage equivariance and the observations entering or leaving a finite burden window then give concrete measurement implications.

DEFINITION A1 (Clock action). *A query $Q : \mathcal{X} \to \mathcal{Z}$ admits a clock action when a group action $\{\rho_u : u \in \mathbb{Z}\}$ satisfies*

$$Q(S_u x) = \rho_u(Q(x)) \tag{A15}$$

for every path and displacement in the maintained translation-stable domain.

For a continuous linear vector query q with matrix action R_q, averaging gives $q(A_p\tau) = \mathbb{E}_p[R_q(U)]q(\tau)$ whenever the expectation and linear map commute. Temporal moments use the Pascal matrix in (22). Nonlinear queries below retain the realized translation and its support.

The population relation (13) averages clock displacements. Pathwise analysis keeps the realized displacement. For an observed path x^W and displacement support $\Gamma \subseteq \mathbb{Z}$, define the latent-path orbit

$$\mathcal{O}_\Gamma(x^W) = \{S_{-u}x^W : u \in \Gamma\}. \tag{A16}$$

PROPOSITION A3 (Clock-orbit identification). *Suppose $x^G \in \mathcal{X}$, $x^W = S_U x^G$, and $U \in \Gamma$. If Q admits the clock action in Definition A1, then*

$$\mathcal{I}_Q(x^W, \Gamma) = Q\Big(\mathcal{O}_\Gamma(x^W)\Big) = \Big\{\rho_{-u}\Big(Q(x^W)\Big) : u \in \Gamma\Big\}. \tag{A17}$$

PROOF. For each $u \in \Gamma$, the latent path associated with that displacement is $S_{-u}x^W$. Apply (A15) to each path in $\mathcal{O}_\Gamma(x^W)$. □

A translation-invariant query has ρ_u equal to the identity action on its value space. For linear queries on $\ell^1(\mathbb{Z})$, this property can be read from the loading sequence.

PROPOSITION A4 (Shift-invariant linear queries). *Let $S \subseteq \mathbb{Z}$ be a set of admissible deterministic clock errors, and let $L_a(x) = \sum_h a_h x_h$ for $a \in \ell^\infty(\mathbb{Z})$. The value $L_a(S_u x)$ is the same for every $u \in S$ and every $x \in \ell^1(\mathbb{Z})$ exactly when*

$$a_{j+u} = a_{j+v} \qquad \text{for every } j \in \mathbb{Z} \text{ and } u, v \in S. \tag{A18}$$

If the subgroup generated by $S - S$ equals $\mathbb{Z}$, then a_h is constant across h, and L_a is a scalar multiple of full-axis cumulative response.

B.1.1. First passage

Let $x = (r, y)$ contain a replacement path $r(h)$ and an activity path $y(h)$. Let $\overline{\mathbb{Z}} = \mathbb{Z} \cup \{-\infty, +\infty\}$, extend integer translation by $(\pm\infty) - u = \pm\infty$, and set $\inf \varnothing = +\infty$. For $\zeta = (q, p, \kappa)$, define the unrestricted first-passage query with values in $\overline{\mathbb{Z}}$

$$D_\zeta(x) = \inf\{h \in \mathbb{Z} : r(h+s) \geq q,\ \ y(h+s) \geq \kappa,\ \ s = 0, \ldots, p-1\}. \tag{A19}$$

The infimum is taken on a translation-stable observation domain; finite-window reporting is handled after this query is formed.

COROLLARY A1 (First-passage clock action). *For every integer u,*

$$D_\zeta(S_u x) = D_\zeta(x) - u. \tag{A20}$$

Hence $\rho_u(d) = d - u$, and Proposition A3 gives

$$\mathcal{I}_{D_\zeta}(x^W, \Gamma) = D_\zeta(x^W) + \Gamma. \tag{A21}$$

If $D_\zeta^W = D_\zeta(x^W)$ and $D_\zeta^G = D_\zeta(x^G)$ are integrable across units, then

$$\mathbb{E}[D_\zeta^G] = \mathbb{E}[D_\zeta^W] + \mathbb{E}[U]. \tag{A22}$$

For finite first-passage values, a pair of endpoint definitions ζ and ζ' yields an origin-free difference:

$$D_{\zeta'}(S_u x) - D_{\zeta}(S_u x) = D_{\zeta'}(x) - D_{\zeta}(x). \tag{A23}$$

Equation (A23) supplies a crossed clock-by-query restriction. A nonzero mixed difference across two recorded origins records changes in measurement ingredients beyond a pure origin shift.

B.1.2. Finite-horizon burden

Let $b_x(h) \in [0, B]$ be a translation-covariant shortfall path, so $b_{S_u x}(h) = b_x(h + u)$, and define

$$\Xi_H(x) = \sum_{h=0}^{H} b_x(h). \tag{A24}$$

PROPOSITION A5 (Boundary sensitivity of cumulative burden). *For every integer u,*

$$\Xi_H(S_u x) - \Xi_H(x) = \begin{cases} \sum_{j=1}^{u} b_x(H+j) - \sum_{j=0}^{u-1} b_x(j), & u > 0, \\ 0, & u = 0, \\ \sum_{j=u}^{-1} b_x(j) - \sum_{j=H+u+1}^{H} b_x(j), & u < 0. \end{cases} \tag{A25}$$

Consequently,

$$|\Xi_H(S_u x) - \Xi_H(x)| \le B|u|. \tag{A26}$$

For the normalized burden $\bar{\Xi}_H = \Xi_H/(H+1)$,

$$\left|\bar{\Xi}_H(S_u x) - \bar{\Xi}_H(x)\right| \le \frac{B|u|}{H+1}. \tag{A27}$$

If $\sum_{h \in \mathbb{Z}} b_x(h) < \infty$, the full-axis burden $\Xi_{\mathbb{Z}}(x) = \sum_{h \in \mathbb{Z}} b_x(h)$ satisfies $\Xi_{\mathbb{Z}}(S_u x) = \Xi_{\mathbb{Z}}(x)$.

B.1.3. Several records for one event

Several recorded clocks can be reconciled by requiring their reindexed paths to agree for a common latent origin. The joint orbit, its query image, and the compatibility equations retain a fixed target intervention, physical path, endpoint, and observation domain.

B.2. Clock-orbit identification

Detailed proof of Proposition A3. For a realized displacement $u \in \Gamma$, equation (7) gives $x^G = S_{-u}x^W$. The set of latent paths generated by Γ is therefore $\mathcal{O}_\Gamma(x^W)$. Applying the query action gives

$$Q(S_{-u}x^W) = \rho_{-u}(Q(x^W)). \tag{A28}$$

Taking the image over $u \in \Gamma$ gives (A17). □

B.3. Shift-invariant linear queries

Proof of Proposition A4. For a deterministic shift u,

$$L_a(S_u x) = \sum_h a_h x_{h+u} = \sum_j a_{j-u} x_j. \tag{A29}$$

Equality across two shifts $u, v \in S$ for every $x \in \ell^1$ is equivalent to $a_{j-u} = a_{j-v}$ for every j. Reindexing gives (A18). The coefficients are invariant under every element of the subgroup generated by $S - S$. If this subgroup is $\mathbb{Z}$, all coefficients are equal. □

B.4. First passage

Proof of Corollary A1. For $S_u x$, the endpoint conditions at recorded horizon h are

$$r(h+u+s) \geq q, \qquad y(h+u+s) \geq \kappa, \qquad s = 0, \ldots, p-1. \tag{A30}$$

Thus h qualifies for $S_u x$ exactly when $h+u$ qualifies for x. Taking infima gives $D_\zeta(S_u x) = D_\zeta(x) - u$. Substitution into Proposition A3 gives (A21). The pathwise identity $D_\zeta^W = D_\zeta^G - U$ gives (A22) after taking expectations. □

Equation (A23) follows by applying (A20) to both endpoint definitions and subtracting.

B.5. Finite-horizon burden

Proof of Proposition A5. Reindex the shifted burden:

$$\Xi_H(S_u x) = \sum_{h=0}^{H} b_x(h+u) = \sum_{j=u}^{H+u} b_x(j). \tag{A31}$$

For $u > 0$, subtracting $\sum_{j=0}^{H} b_x(j)$ leaves the u observations entering above H and removes the u observations starting at zero. For $u < 0$, it adds the observations from u through -1 and removes the observations from $H+u+1$ through H. This gives (A25). Since each term

TABLE A1. Clock action by query family

Query	Transformation under S_u	Timing object entering recovery
Full-axis cumulative mass T_0	$T_0(S_u x) = T_0(x)$	Probability normalization
Temporal moments $T_0, \dots, T_r$	$\mathbf{T}_r(S_u x) = \Pi_r(u)\mathbf{T}_r(x)$	Clock moments through order r
First passage D_ζ	$D_\zeta(S_u x) = D_\zeta(x) - u$	Displacement support or moments
Finite burden Ξ_H	Boundary formula (A25)	Displacement and boundary path
Full-axis burden $\Xi_{\mathbb{Z}}$	$\Xi_{\mathbb{Z}}(S_u x) = \Xi_{\mathbb{Z}}(x)$	Translation action
Point response $x(h)$	$(S_u x)(h) = x(h+u)$	Clock displacement

The table records deterministic translation laws. Population averaging over a random U produces the corresponding average-clock objects.

lies in $[0, B]$, the absolute difference is bounded by $B|u|$, which gives (A26); division by $H + 1$ gives (A27). For the full-axis burden, absolute summability permits reindexing:

$$\Xi_{\mathbb{Z}}(S_u x) = \sum_{h \in \mathbb{Z}} b_x(h+u) = \sum_{k \in \mathbb{Z}} b_x(k) = \Xi_{\mathbb{Z}}(x). \tag{A32}$$

□

B.6. Multiple recorded clocks

Suppose J recorded origins satisfy $x^{W_j} = S_{U_j} x^G$, and let the joint displacement vector $U = (U_1, \dots, U_J)$ belong to $\Gamma \subseteq \mathbb{Z}^J$. For the recorded path vector $\mathbf{x}^W = (x^{W_1}, \dots, x^{W_J})$, define the common latent-path orbit

$$\mathcal{O}_\Gamma^{(J)}(\mathbf{x}^W) = \left\{ x \in \mathcal{X} : \exists u \in \Gamma \text{ such that } x = S_{-u_j} x^{W_j} \text{ for every } j \right\}. \tag{A33}$$

PROPOSITION A6 (Query set across clocks). *For any query Q,*

$$\mathcal{I}_Q^{(J)}(\mathbf{x}^W, \Gamma) = Q\Big(\mathcal{O}_\Gamma^{(J)}(\mathbf{x}^W)\Big). \tag{A34}$$

If Q admits the clock action ρ and $q_j = Q(x^{W_j})$, then

$$\mathcal{I}_Q^{(J)} = \left\{ q : \exists u \in \Gamma,\ q = \rho_{-u_j}(q_j) \textit{ for every } j,\ S_{-u_j} x^{W_j} = S_{-u_k} x^{W_k} \textit{ for every } j, k \right\}. \tag{A35}$$

For first passage, (A35) requires a common value $d = D_\zeta(x^{W_j}) + u_j$ across recorded clocks together with a common reindexed path. The first-passage query translates by the clock displacement. The finite-horizon burden changes through observations entering and leaving the window. The full-axis burden is translation invariant. Table A1 collects these transformation laws together with the temporal-moment action.

Proof of Proposition A6. A path x belongs to $\mathcal{O}_{\Gamma}^{(J)}(\mathbf{x}^W)$ exactly when there is a displacement vector $u \in \Gamma$ with $x = S_{-u_j} x^{W_j}$ for every j. Applying Q to this set gives (A34). If Q admits the action ρ, then each common path satisfies

$$Q(x) = Q(S_{-u_j} x^{W_j}) = \rho_{-u_j}(q_j) \tag{A36}$$

for every j. Conversely, a vector u satisfying the query equalities and the common-path equalities in (A35) defines an element of $\mathcal{O}_{\Gamma}^{(J)}(\mathbf{x}^W)$ whose query value is q. This gives (A35). □

Appendix C. Linear Query Identification

The operator foundations of Carrasco et al. (2007) and the functional-identification framework of Severini and Tripathi (2006); Santos (2011); Severini and Tripathi (2012) yield Proposition A7, the Hilbert-space null-space/range characterization. The spectral corollary is its translation-clock specialization, and the variance-minimizing bridge uses generalized least squares.

C.1. Query identification

PROPOSITION A7 (Linear query characterization). *For $a \in \mathcal{H}$, the query $\psi_a(\tau) = \langle a, \tau\rangle_{\mathcal{H}}$ is constant on each fiber $\{\tau : A\tau = m\}$ exactly when*

$$a \in \ker(A)^{\perp} = \overline{\mathrm{Range}(A^*)}. \tag{A37}$$

A representation $\psi_a(\tau) = \langle b, m\rangle_{\mathcal{Y}}$ by a bounded linear functional on $\mathcal{Y}$ exists exactly when

$$a \in \mathrm{Range}(A^*). \tag{A38}$$

Each b satisfying $A^*b = a$ is a bridge for the query. When $\mathrm{Range}(A^*)$ *is closed,* $\ker(A)^{\perp} = \mathrm{Range}(A^*)$*, so every identified linear query has a bridge representation.*

Proof of Proposition A7. Suppose $a \in \ker(A)^{\perp}$. If $A\tau_1 = A\tau_2$, then $\tau_1 - \tau_2 \in \ker(A)$, so $\langle a, \tau_1 - \tau_2\rangle = 0$. Hence the query is constant on the solution set. Conversely, if a has a component along $\ker(A)$, choose $v \in \ker(A)$ with $\langle a, v\rangle \neq 0$. The paths τ and $\tau + v$ generate the same m and different query values. For bounded operators between Hilbert spaces, $\ker(A)^{\perp} = \overline{\mathrm{Range}(A^*)}$. If $a = A^*b$, then $\langle a, \tau\rangle = \langle b, A\tau\rangle = \langle b, m\rangle$. Conversely, suppose the query equals a bounded linear functional of m on $\mathcal{Y}$. The Riesz representation theorem gives $b \in \mathcal{Y}$ such that $\langle a, \tau\rangle = \langle b, A\tau\rangle = \langle A^*b, \tau\rangle$ for every τ, hence $a = A^*b$. □

C.2. Spectral identification

Fourier multiplication is the deconvolution representation; Zinde-Walsh (2014) develops identification and well-posedness in generalized-function spaces. Here the maintained spaces are $\ell^2(\mathbb{Z})$ and $L^2[-\pi,\pi]$. Use the Fourier transform $\widehat{f}(\omega) = \sum_h f_h e^{-i\omega h}$. Proposition A1 gives

$$\widehat{m}(\omega) = \phi_U(\omega)\widehat{\tau}(\omega), \qquad \phi_U(\omega) = \mathbb{E}[e^{i\omega U}]. \tag{A39}$$

COROLLARY A2 (Spectral identification). *The complete path has one value when $\phi_U(\omega)$ is nonzero almost everywhere. A query $a \in \ell^2(\mathbb{Z})$ has one value when $\widehat{a}(\omega)$ vanishes on the zero set of ϕ_U, up to sets of measure zero. A bounded bridge exists when*

$$\frac{\widehat{a}(\omega)}{\overline{\phi_U(\omega)}} \in L^2[-\pi,\pi]. \tag{A40}$$

PROOF OF COROLLARY A2. The Fourier transform is a unitary map from $\ell^2(\mathbb{Z})$ to $L^2[-\pi,\pi]$. Under this map, the clock operator is multiplication by ϕ_U. Its null space consists of functions whose Fourier transforms are supported on the zero set of ϕ_U. The complete path has one value exactly when this null space contains only zero, which holds when the zero set has Lebesgue measure zero. A query belongs to the orthogonal complement of this null space exactly when its Fourier transform vanishes on the zero set. The adjoint multiplier is $\overline{\phi_U}$. The equation $A^*b = a$ therefore has an L^2 solution exactly when $\widehat{a}/\overline{\phi_U} \in L^2$. □

C.3. Triangulation

Suppose J clocks produce $m_j = A_j\tau$. Define the stacked operator $A_\oplus\tau = (A_1\tau,\ldots,A_J\tau)$.

PROPOSITION A8 (Identification from multiple clocks). *The stacked null space satisfies*

$$\ker(A_\oplus) = \bigcap_{j=1}^{J} \ker(A_j). \tag{A41}$$

A query a has one value under the joint clock system exactly when a is orthogonal to this intersection. The complete response path has one value when the intersection contains only the zero element.

PROOF OF PROPOSITION A8. The equality $A_\oplus v = 0$ holds exactly when $A_j v = 0$ for every j. Hence $\ker(A_\oplus) = \cap_j \ker(A_j)$. Apply Proposition A7 to the stacked operator. □

C.4. Optimal known-clock bridge

LEMMA A2 (Weighted bridge solution). *Let Ω be positive definite and suppose $a \in \mathrm{Range}(A^\top)$. The solution to*

$$\min_b b^\top \Omega b \quad \textit{subject to} \quad A^\top b = a \tag{A42}$$

is $b^* = \Omega^{-1}A(A^\top\Omega^{-1}A)^+ a$.

PROOF. Set $c = \Omega^{1/2}b$. The problem becomes minimum Euclidean norm subject to $A^\top\Omega^{-1/2}c = a$. The Moore–Penrose solution is $c^* = (A^\top\Omega^{-1/2})^+ a$. Transforming back gives the displayed formula. Substitution verifies the constraint, and the projection property gives minimal norm. □

C.5. Variance factor

For a first-stage covariance Ω/n, the finite-dimensional bridge has variance $b^\top\Omega b/n$. Substituting the preceding solution yields

$$v_A(a) = a^\top(A^\top\Omega^{-1}A)^+ a. \tag{A43}$$

The known-clock calculation conditions on A, and the estimated-clock calculation adds its estimation uncertainty.

Appendix D. Cohort Heterogeneity and Clock Mixing

D.1. Latent cohort mixing

Let $\mathcal{G}$ be a finite set of latent treatment cohorts and $\mathcal{W}$ a finite set of recorded clock cells. Define

$$Q_{wg} = \mathbb{P}(G_i = g \mid W_i = w). \tag{A44}$$

For each calendar time t, let $\theta_{g,t}$ be the group-time effect in (3). Let $m_{w,t}$ denote the causal contrast for clock cell w after removal of the untreated counterfactual.

ASSUMPTION A1 (Cohort-cell clock condition). *For every g, w, t with positive cell probability,*

$$\mathbb{E}[Y_{it}(g) - Y_{it}(\infty) \mid G_i = g, W_i = w] = \theta_{g,t}. \tag{A45}$$

PROPOSITION A9 (Clock mixing). *Under Assumption A1,*

$$m_{w,t} = \sum_{g \in \mathcal{G}} Q_{wg} \theta_{g,t}. \tag{A46}$$

Writing $m_t = Q\theta_t$, a cohort query $c^\top \theta_t$ has one value exactly when $c \in \mathrm{Range}(Q^\top)$.

Equation (A46) separates cohort heterogeneity from clock mixing. The matrix Q can come from linked administrative records, a validation sample, or a maintained timing model.

D.2. Baselines under interval timing

Suppose unit i has interval timing information $G_i \in [\underline{G}_i, \overline{G}_i]$. Proposition 1 supplies a recorded-horizon causal contrast from a baseline $r_i < \underline{G}_i$ and an identified untreated change. For clock cell w, the same construction yields $m_{w,t}$. Proposition A9 then maps that causal contrast into latent cohort effects through Q_{wg}.

PROOF OF PROPOSITION A9. Iterated expectation gives

$$m_{w,t} = \sum_g \mathbb{P}(G_i = g \mid W_i = w)\mathbb{E}[Y_{it}(g) - Y_{it}(\infty) \mid G_i = g, W_i = w] \tag{A47}$$

$$= \sum_g Q_{wg} \theta_{g,t}, \tag{A48}$$

where the second equality uses Assumption A1. The query statement follows from Proposition A7 applied to the finite matrix Q. □

D.3. Conditional cells and pooled response

Let $G_i = 0$, let $X_i \in \{0, 1\}$ have equal probabilities, and let $U_i = X_i$. Set $\tau_{i,h} = (1 + X_i)\mathbf{1}\{h = 0\}$. Within a cell defined by G_i and X_i, the response mean is invariant across the recorded-clock support, which has one value. In the pooled population the mean latent response has mass 3/2 at horizon zero. The recorded mean has masses

$$m_{-1} = 1, \qquad m_0 = \frac{1}{2}, \tag{A49}$$

and zero elsewhere. Applying the pooled marginal clock to the pooled mean response gives masses 3/4 at each of these horizons. Thus conditional mixing retains the association between the cell's response and its clock law.

$$T_0 = \frac{3}{2}, \qquad T_1 = 0, \qquad M_1 = -1, \qquad \mu_1 = \frac{1}{2}, \qquad \mathrm{Cov}(U_i, T_{0i}) = \frac{1}{4}. \tag{A50}$$

Equation (39) recovers $T_1 = -1 + (1/2)(3/2) + 1/4 = 0$. This finite construction demonstrates the aggregation condition. The unit-response quantities in this illustration are specified potential-outcome contrasts; an empirical implementation obtains such contrasts under its causal design.

Appendix E. Estimated Clock Operator

Unknown-operator estimation is studied in inverse-problem settings. Johannes et al. (2011) derive nonparametric rates under regularity and operator-link conditions. Kato and Sasaki (2018) construct density bands using an auxiliary error sample; Kato et al. (2021) use repeated-measurement moment restrictions for inference with partial identification. Functional estimation has query-specific regularity and rates (Santos 2011; Breunig and Johannes 2016). A differentiable finite-dimensional validation model and an asymptotically linear first stage yield the representative-invariance condition for the clock derivative and local query membership needed for differentiable selection in the delta method.

A validation sample can link a recorded timing signal to a latent or higher-resolution timing measure. Let $\eta \in \mathbb{R}^q$ index the clock operator implied by that validation model. The causal sample supplies $\widehat{m}$, and the validation sample supplies $\widehat{\eta}$ and its covariance.

TABLE A2. Clock-information regimes

Clock regime	Timing input supplied by the analysis	Statistical object
Known clock	A, moments, or displacement support	Query equation from Table 2
Estimated clock	$\widehat{\eta}$, V_η, and $A(\eta)$	Stable-bridge variance
Operator sequence	A_n and Ω_n	Bridge variance and projection set
Clock-law set	$\mathcal{P}$ and response restrictions $\mathcal{T}$	Attainable query set

Query type and clock-information regime form separate coordinates. A given query can be studied under each regime supported by the data and maintained model.

E.1. Finite-moment scheduling derivatives

For g in (45), write $a = M_1/M_0 + \mu_1$ and $v = M_2/M_0 - (M_1/M_0)^2 - \mu_2 + \mu_1^2$. On $M_0 > 0$, the two Jacobian rows are

$$Da = \left(-\frac{M_1}{M_0^2}, \frac{1}{M_0}, 0, 1, 0\right), \tag{A51}$$

$$Dv = \left(-\frac{M_2}{M_0^2} + \frac{2M_1^2}{M_0^3}, -\frac{2M_1}{M_0^2}, \frac{1}{M_0}, 2\mu_1, -1\right). \tag{A52}$$

Ordinary differentiation gives these expressions. A joint central limit theorem for the five input estimates yields the covariance used in the implementation. The sampling law and its consistent covariance estimate are supplied by the response and validation designs. A clock law imposed as a sensitivity specification is treated as a fixed input to this calculation.

E.2. The provision-cost contrast and its uncertainty

This calculation specializes the smooth finite-moment map to the economic decision. With $D = M_2 - M_1^2/M_0 - M_0(\mu_2 - \mu_1^2)$, equation (47) is $\Delta = \gamma D - K$. Its derivative with respect to $z = (M_0, M_1, M_2, \mu_1, \mu_2)$ is

$$\nabla_z \Delta = \gamma \left(\frac{M_1^2}{M_0^2} - \mu_2 + \mu_1^2,\ -\frac{2M_1}{M_0},\ 1,\ 2M_0\mu_1,\ -M_0 \right)^{\top}. \tag{A53}$$

Differentiating with respect to γ and K gives D and -1. Under the stated joint CLT and positive-mass conditions, the asymptotic variance is the quadratic form of this full gradient and the joint input covariance. The n/n_v factor in equation (46) converts validation uncertainty to the response-sample normalization. Overlapping samples retain their cross-covariance. These are consequences of the supplied joint CLT, and place no new root-n assertion on a particular first-stage estimator.

For completeness, if a denotes the relevant full gradient and only the marginal asymptotic standard deviations s_j of the inputs are known, every covariance matrix Σ with these diagonal entries satisfies

$$a^{\top}\Sigma a \ \le\ \left(\sum_j |a_j| s_j \right)^2 . \tag{A54}$$

Positive semidefiniteness gives $|\Sigma_{jk}| \le s_j s_k$; expanding the quadratic form proves the inequality. It is attained over the unrestricted covariance class by $\Sigma_{jk} = s_j s_k \operatorname{sgn}(a_j) \operatorname{sgn}(a_k)$, with arbitrary signs at zero coordinates. This is the elementary worst-correlation calculation used in calibration inference by Cocci and Plagborg-Møller (2025, Lemma 1). Known sampling restrictions can reduce the class and the bound. A marginal standard-error list therefore has a different interpretation from an assumption of independent inputs. The empirical gas calculations retain their original covariance procedures.

E.3. Stable bridges

Let $A(\eta) \in \mathbb{R}^{J\times H}$ be differentiable in η. Write $A_0 = A(\eta_0)$ and

$$A_j = \left.\frac{\partial A(\eta)}{\partial \eta_j}\right|_{\eta=\eta_0}, \qquad j = 1, \ldots, q. \tag{A55}$$

The population causal moment satisfies $m = A_0\tau$, and the query is $\psi = a^\top \tau$.

DEFINITION A2 (Stable bridge). *A vector $b \in \mathbb{R}^J$ is a stable bridge for a when*

$$A_0^\top b = a, \qquad A_j^\top b \in \mathrm{Range}(A_0^\top) \quad \text{for } j = 1, \ldots, q. \tag{A56}$$

The stable dual space is $\mathcal{S} = \{b : A_j^\top b \in \mathrm{Range}(A_0^\top),\ j = 1, \ldots, q\}$, and the stable bridge set for query a is $\mathcal{B}_s(a) = \{b \in \mathcal{S} : A_0^\top b = a\}$.

The first condition identifies the query conditional on the clock. The remaining conditions identify the first-order sensitivity of that query to each clock direction. A bridge b admits a local bridge path when there is a neighborhood $\mathcal{N}_b$ of η_0 and a continuously differentiable map $\beta_b : \mathcal{N}_b \to \mathbb{R}^J$ satisfying $\beta_b(\eta_0) = b$ and $A(\eta)^\top \beta_b(\eta) = a$ throughout $\mathcal{N}_b$.

E.4. Observable clock sensitivity

Let R_0 be any right inverse on $\mathrm{Range}(A_0)$, so $A_0 R_0 m = m$. Define

$$\Gamma_m(b) = \left(b^\top A_1 R_0 m, \ldots, b^\top A_q R_0 m\right)^\top. \tag{A57}$$

ASSUMPTION A2 (Local bridge selection). *Every $b \in \mathcal{B}_s(a)$ admits a local bridge path. The learned-clock estimator associated with b evaluates $\beta_b(\hat{\eta})^\top \hat{m}$.*

PROPOSITION A10 (Rank condition for local bridge selection). *Suppose $A(\eta)$ is continuously differentiable on a neighborhood $\mathcal{N}$ of η_0, $\operatorname{rank} A(\eta)$ is constant on $\mathcal{N}$, and $a \in \mathrm{Range}(A(\eta)^\top)$ for every $\eta \in \mathcal{N}$. Then Assumption A2 holds. For $b \in \mathcal{B}_s(a)$, one bridge path is*

$$\beta_b(\eta) = (A(\eta)^+)^\top a + \{I_J - A(\eta)A(\eta)^+\}\left\{b - (A_0^+)^\top a\right\}. \tag{A58}$$

The construction uses differentiability of the Moore–Penrose inverse on a constant-rank neighborhood (Golub and Pereyra 1973). In that neighborhood, if query membership holds, the same formula extends every base bridge satisfying $A_0^\top b = a$. Lemma A4 then implies stability for every such bridge. Thus, in this regular regime the stability restriction is implied by local identification.

First-order stability alone concerns a derivative at the reference model. For example, take $A(\eta) = (1, \eta^2)$, $a = (1, 0)^\top$, $\eta_0 = 0$, and $b = 1$. The rank equals one throughout, and

$A_0' = 0$ makes b stable at zero. For each $\eta \neq 0$, query membership fails: the first component of $A(\eta)^\top \beta = a$ forces $\beta = 1$, and the second requires $\eta^2 = 0$. This example locates the separate local-membership requirement. For a parametric validation model, rank can be tracked through singular values, and query membership through

$$r_a(\eta) = \left\| \{I_H - A(\eta)^+ A(\eta)\} a \right\| . \tag{A59}$$

A maintained neighborhood with constant rank and $r_a(\eta) = 0$ supplies the local selection used by the plug-in calculation.

THEOREM A1 (Inference with an estimated clock operator). *For every stable bridge b, the vector $\Gamma_m(b)$ is invariant to the choice of R_0 and satisfies*

$$\Gamma_m(b) = \left(b^\top A_1 \tau, \ldots, b^\top A_q \tau\right)^\top . \tag{A60}$$

Let $\widehat{m}$ and $\widehat{\eta}$ be asymptotically linear estimators from independent samples of sizes n and N, with $N/n \to \rho \in (0, \infty)$, finite influence covariances Ω_m and V_η, and the corresponding joint Gaussian limit. Under Assumption A2, define

$$\widetilde{D}(m) = \left[A_1 A_0^+ m, \ldots, A_q A_0^+ m\right] . \tag{A61}$$

The learned-clock estimator has first-order variance

$$V(b) = b^\top \Omega_m b + \rho^{-1} \Gamma_m(b)^\top V_\eta \Gamma_m(b) = b^\top \Omega_{\mathrm{FC}}^{\mathrm{obs}} b, \tag{A62}$$

where

$$\Omega_{\mathrm{FC}}^{\mathrm{obs}} = \Omega_m + \rho^{-1} \widetilde{D}(m) V_\eta \widetilde{D}(m)^\top . \tag{A63}$$

The quadratic form in (A62) *is invariant across right-inverse representatives on the stable bridge space.*

E.5. Optimal stable bridge

Let N_0 be a matrix whose columns span $\ker(A_0)$, and set

$$C = \left[A_1 N_0, \ldots, A_q N_0\right], \qquad L = [A_0, C], \qquad d = (a^\top, 0^\top)^\top . \tag{A64}$$

The stable constraints are $L^\top b = d$.

COROLLARY A3 (Optimal stable bridge). *Suppose the stable bridge set is nonempty and* $\Omega^{\text{obs}}_{\text{FC}}$ *is positive definite. The bridge minimizing* (A62) *is*

$$b^*_{\text{st}} = (\Omega^{\text{obs}}_{\text{FC}})^{-1} L \left[L^\top (\Omega^{\text{obs}}_{\text{FC}})^{-1} L\right]^+ d. \tag{A65}$$

The minimum variance is

$$V^*_{\text{st}} = d^\top \left[L^\top (\Omega^{\text{obs}}_{\text{FC}})^{-1} L\right]^+ d. \tag{A66}$$

The learned-clock query space is $A_0^\top \mathcal{S}$. It is contained in $\text{Range}(A_0^\top)$, the query space conditional on a known clock.

E.6. Stable bridge characterization

LEMMA A3 (Stability equivalence). *For* $b \in \mathbb{R}^J$*, the following statements are equivalent for each* j*:* $A_j^\top b \in \text{Range}(A_0^\top)$*;* $b^\top A_j v = 0$ *for every* $v \in \ker(A_0)$*;* $(A_j N_0)^\top b = 0$ *for a basis matrix* N_0 *of* $\ker(A_0)$.

PROOF. Finite-dimensional orthogonality gives $\text{Range}(A_0^\top) = \ker(A_0)^\perp$. The second and third statements express orthogonality to the same subspace. □

LEMMA A4 (Local bridge path implies stability). *Let* b *satisfy* $A_0^\top b = a$*. If there is a neighborhood of* η_0 *and a continuously differentiable map* β_b *satisfying* $\beta_b(\eta_0) = b$ *and* $A(\eta)^\top \beta_b(\eta) = a$ *on that neighborhood, then* b *satisfies Definition A2.*

PROOF. Differentiate $A(\eta)^\top \beta_b(\eta) = a$ with respect to η_j at η_0. The derivative satisfies $A_j^\top b + A_0^\top \dot\beta_{b,j} = 0$, so $A_j^\top b = -A_0^\top \dot\beta_{b,j} \in \text{Range}(A_0^\top)$ for every j. □

PROOF OF PROPOSITION A10. Constant rank and continuous differentiability imply continuous differentiability of $A(\eta)^+$ on $\mathcal{N}$. Query membership gives $A(\eta)^\top (A(\eta)^+)^\top a = a$. For $z_0 = b - (A_0^+)^\top a$, the bridge equation at η_0 gives $z_0 \in \ker(A_0^\top)$, so $\{I_J - A_0 A_0^+\} z_0 = z_0$. For every η, the matrix $I_J - A(\eta)A(\eta)^+$ projects onto $\ker(A(\eta)^\top)$. Equation (A58) is therefore continuously differentiable, equals b at η_0, and satisfies $A(\eta)^\top \beta_b(\eta) = a$ throughout $\mathcal{N}$. □

E.7. Observable sensitivity

DETAILED PROOF OF THEOREM A1. Let R_0 satisfy $A_0 R_0 m = m$. Since $m = A_0 \tau$,

$$A_0(\tau - R_0 m) = 0, \tag{A67}$$

so $\tau = R_0 m + v$ for some $v \in \ker(A_0)$. For a stable bridge, Lemma A3 gives $b^\top A_j v = 0$, and therefore

$$b^\top A_j \tau = b^\top A_j R_0 m. \tag{A68}$$

This identity proves (A60). If R_1 is another right inverse on the range, then $(R_0 - R_1)m \in \ker(A_0)$, so the same stability argument gives right-inverse invariance. For the influence expansion, let

$$\sqrt{n}(\widehat{m} - m) = \frac{1}{\sqrt{n}} \sum_{i=1}^{n} \xi_i + o_p(1), \tag{A69}$$

$$\sqrt{N}(\widehat{\eta} - \eta_0) = \frac{1}{\sqrt{N}} \sum_{j=1}^{N} \zeta_j + o_p(1). \tag{A70}$$

Assumption A2 supplies the differentiable map $\beta_b(\eta)$. Differentiation gives

$$A_j^\top b + A_0^\top \dot{\beta}_{b,j} = 0. \tag{A71}$$

Since $m = A_0 \tau$,

$$\dot{\beta}_{b,j}^\top m = \tau^\top A_0^\top \dot{\beta}_{b,j} = -\tau^\top A_j^\top b = -b^\top A_j \tau = -\Gamma_m(b)_j. \tag{A72}$$

A first-order expansion yields

$$\sqrt{n}(\widehat{\psi} - \psi) = \frac{1}{\sqrt{n}} \sum_{i=1}^{n} b^\top \xi_i - \rho^{-1/2} \frac{1}{\sqrt{N}} \sum_{j=1}^{N} \Gamma_m(b)^\top \zeta_j + o_p(1). \tag{A73}$$

Independence of the samples gives

$$V(b) = b^\top \Omega_m b + \rho^{-1} \Gamma_m(b)^\top V_\eta \Gamma_m(b). \tag{A74}$$

Using the Moore–Penrose representative $A_0^+ m$ yields $\Gamma_m(b) = \widetilde{D}(m)^\top b$ on the stable bridge space, which gives (A63). ☐

E.8. Optimal stable bridge

PROOF OF COROLLARY A3. Lemma A3 gives the constraints $A_0^\top b = a$ and $C^\top b = 0$, or $L^\top b = d$. Apply Lemma A2 with A replaced by L, a replaced by d, and Ω replaced by $\Omega_{\mathrm{FC}}^{\mathrm{obs}}$. The objective equals the first-order variance on the feasible set by Theorem A1. ☐

E.9. Same-sample extension

Suppose the causal moment and clock parameter are estimated from a common sample. Let $\Sigma_{m\eta} = \mathrm{Cov}(\xi, \zeta)$. The influence function is $b^\top \xi - \Gamma_m(b)^\top \zeta$, so

$$V_{\mathrm{same}}(b) = b^\top \Omega_m b + \Gamma_m(b)^\top V_\eta \Gamma_m(b) - 2b^\top \Sigma_{m\eta} \Gamma_m(b). \tag{A75}$$

Since $\Gamma_m(b) = \widetilde{D}(m)^\top b$ on the stable space,

$$V_{\mathrm{same}}(b) = b^\top \left\{ \Omega_m + \widetilde{D} V_\eta \widetilde{D}^\top - \Sigma_{m\eta} \widetilde{D}^\top - \widetilde{D} \Sigma_{m\eta}^\top \right\} b. \tag{A76}$$

The same constrained quadratic program applies with this covariance matrix.

E.10. A local regularity condition

The stable bridge restriction has a pathwise interpretation. Let $h \in \mathbb{R}^q$ be a clock tangent and write $\dot{A}[h] = \sum_j h_j A_j$. Suppose $v \in \ker(A_0)$ and $\dot{A}[h]v \in \mathrm{Range}(A_0)$. Choose δ with $A_0 \delta = -\dot{A}[h]v$. The paths $(\eta_0 + th, \tau_0)$ and $(\eta_0 + th, \tau_0 + v + t\delta)$ have the same observed-moment derivative at $t = 0$. Their query derivatives differ by

$$a^\top \delta = -b^\top \dot{A}[h] v. \tag{A77}$$

A stable bridge makes this difference equal to zero for every such h, v. A nonzero value produces two observationally equivalent first-order paths with different query derivatives. Definition A2 is a first-order compatibility condition. Assumption A2 supplies the local differentiable bridge selection used by the plug-in estimator. Proposition A10 gives a finite-dimensional route through constant rank and query membership over a neighborhood.

Appendix F. Clock-Operator Sequences and Projection Inference

The calculations below use the Gaussian information bound and projection of a moment confidence region. Functional efficiency bounds are developed by Severini and Tripathi (2012); Santos (2012) and Kaido et al. (2019) study inference on partially identified models and their projections. The calculation uses a Gaussian ellipsoid with known covariance and its own coverage statement. The clock operator indexes the geometry of this experiment.

Consider a sequence of finite-dimensional experiments indexed by n. The population moment is $m_n = A_n \tau_n$, and

$$\sqrt{n}(\widehat{m}_n - m_n) \rightsquigarrow N(0, \Omega_n). \tag{A78}$$

For a query $a_n^\top \tau_n$, define

$$\nu_n(a_n) = \inf_{b:A_n^\top b = a_n} b^\top \Omega_n b, \tag{A79}$$

with value $+\infty$ when the bridge set is empty.

PROPOSITION A11 (Bridge variance in a Gaussian clock experiment). *Suppose Ω_n is positive definite and the bridge set is nonempty. Then*

$$\nu_n(a_n) = a_n^\top (A_n^\top \Omega_n^{-1} A_n)^+ a_n. \tag{A80}$$

In the Gaussian shift experiment, $\nu_n(a_n)/n$ is the information lower bound for regular estimation of $a_n^\top \tau_n$. A bounded sequence $\nu_n(a_n)$ yields bounded root-n variance through the variance-minimizing bridge. A diverging sequence yields a diverging root-n variance bound.

PROOF. The closed form follows from Lemma A2. In the Gaussian shift experiment $\widehat{m}_n \sim N(A_n\tau_n, \Omega_n/n)$, the information matrix for τ_n is $I_n = A_n^\top \Omega_n^{-1} A_n$. The generalized information bound for $a_n^\top \tau_n$ is $a_n^\top I_n^+ a_n/n = \nu_n(a_n)/n$. The variance-minimizing bridge estimator attains this bound. □

The quantity $\nu_n(a_n)$ is indexed by the query loading, clock operator, and causal-moment covariance. A single operator sequence can therefore generate different variance paths across query loadings.

F.1. Projection inference

Let $\widehat{m} \in \mathbb{R}^J$, let Ω be positive definite, and write $\nu_A(a) = a^\top (A^\top \Omega^{-1} A)^+ a$. Define

$$Q_n(\tau) = n(\widehat{m} - A\tau)^\top \Omega^{-1} (\widehat{m} - A\tau). \tag{A81}$$

In the Gaussian model with known Ω, inversion of the J-dimensional moment ellipsoid gives the query set

$$\mathcal{C}_{1-\alpha} = \{a^\top \tau : Q_n(\tau) \le \chi^2_{J,1-\alpha}\}. \tag{A82}$$

Let $\widehat{\tau}$ be a generalized least-squares minimizer and $Q_{\min} = Q_n(\widehat{\tau})$. For an identified query, constrained quadratic minimization gives

$$\inf_{\tau:a^\top \tau = \psi} Q_n(\tau) = Q_{\min} + \frac{n(\psi - a^\top \widehat{\tau})^2}{\nu_A(a)}. \tag{A83}$$

Hence the projection set is

$$a^\top \widehat{\tau} \pm \sqrt{v_A(a)} \sqrt{\frac{\chi^2_{J,1-\alpha} - Q_{\min}}{n}} \tag{A84}$$

whenever $Q_{\min} \le \chi^2_{J,1-\alpha}$. The construction remains defined when the clock operator is singular because optimization is performed over the moment equation and query image.

Appendix G. Clock Laws Specified as a Set

The identified-set construction takes the query image of all environments satisfying the observation equation and maintained restrictions (Tamer 2010; Molinari 2020). Several recorded dates, interval restrictions on timing error, or a validation analysis can define a set $\mathcal{P}$ of clock laws. Response restrictions define a set $\mathcal{T}$. Let $A(p)$ denote the clock operator generated by $p \in \mathcal{P}$. Define

$$\Theta_a(m) = \{a^\top \tau : m = A(p)\tau,\ p \in \mathcal{P},\ \tau \in \mathcal{T}\}. \tag{A85}$$

PROPOSITION A12 (Attainable query set under a clock set). *In the common-response additive-clock model with clock independence, every element of $\Theta_a(m)$ is generated by an admissible data-generating process. Hence $\Theta_a(m)$ equals the identified query set for that maintained class.*

PROOF. Take any pair (p, τ) satisfying $m = A(p)\tau$, $p \in \mathcal{P}$, and $\tau \in \mathcal{T}$. Set $G_i = 0$ for every unit. Draw U_i independently from p, and set $W_i = U_i$. Let $Y_{it}(\infty) = \varepsilon_{it}$ and $Y_{it}(0) = \varepsilon_{it} + \tau_t$, where ε_{it} has mean zero and is independent of U_i. The recorded-clock causal response is $\mathbb{E}[\tau_{\ell+U}] = A(p)\tau = m$, and the query equals $a^\top\tau$. Every feasible query value is attained. □

G.1. Bilinear geometry

The restriction $m = A(p)\tau$ is bilinear in p and τ. A two-point clock with $\mathbb{P}(U = 1) = p$ and a zero pre-event response gives $m_{-1} = p\tau_0$. Fixing $m_{-1} = 1$ yields the feasible curve $p\tau_0 = 1$.

G.2. Fixed-clock shape programs

Fix p and let $\mathcal{T} = \{\tau : C\tau \le d\}$. The lower endpoint of a query solves

$$v_-(p) = \min_\tau a^\top \tau \quad \text{subject to} \quad A(p)\tau = m, \quad C\tau \le d. \tag{A86}$$

When the primal is feasible and has a finite optimum, its linear-program dual is

$$\nu_-(p) = \max_{y\in\mathbb{R}^J,\ z\geq 0} \{y^\top m - z^\top d : A(p)^\top y - C^\top z = a\}. \tag{A87}$$

The vector y is a data bridge and z is the multiplier on the shape restrictions. Nonnegativity, monotonicity, bounded first differences, and discrete curvature restrictions enter through $C\tau \leq d$.

G.3. Candidate clocks and profiling

For a finite set $\mathcal{P} = \{p^{(1)}, \dots, p^{(M)}\}$, define $\nu_+(p)$ by replacing the minimization in (A86) with maximization. Then

$$\Theta_a(m) = \bigcup_{r=1}^{M} [\nu_-(p^{(r)}), \nu_+(p^{(r)})]. \tag{A88}$$

For a low-dimensional family $p(\lambda)$, each λ indexes a fixed-clock program and the outer calculation profiles the endpoint functions over λ.

G.4. Two-point recursion

Suppose $U \in \{0,1\}$, $\mathbb{P}(U=1) = p > 0$, and $\tau_h = 0$ for $h < 0$. Then

$$m_\ell = (1-p)\tau_\ell + p\tau_{\ell+1}. \tag{A89}$$

The latent path is a function of p:

$$\tau_0(p) = \frac{m_{-1}}{p}, \qquad \tau_{h+1}(p) = \frac{m_h - (1-p)\tau_h(p)}{p}. \tag{A90}$$

Shape restrictions select an admissible subset of p, and the query set is the image of that subset under $a^\top\tau(p)$.

Appendix H. Numerical Details

The first numerical example uses latent horizons $-4, \dots, 8$, with $\tau_0 = 2$, $\tau_1 = 4$, $\tau_2 = 3$, $\tau_3 = 2$, $\tau_4 = 1$, and zero elsewhere. The clock law assigns probability one half to $U = 0$ and one half to $U = 2$. The recorded response is $m_\ell = (\tau_\ell + \tau_{\ell+2})/2$. The totals satisfy $\sum_h \tau_h = \sum_\ell m_\ell = 12$. For the spectral figure, the clock characteristic function is

$$\phi_U(\omega) = \frac{1+\exp(2i\omega)}{2} = \exp(i\omega)\cos(\omega), \tag{A91}$$

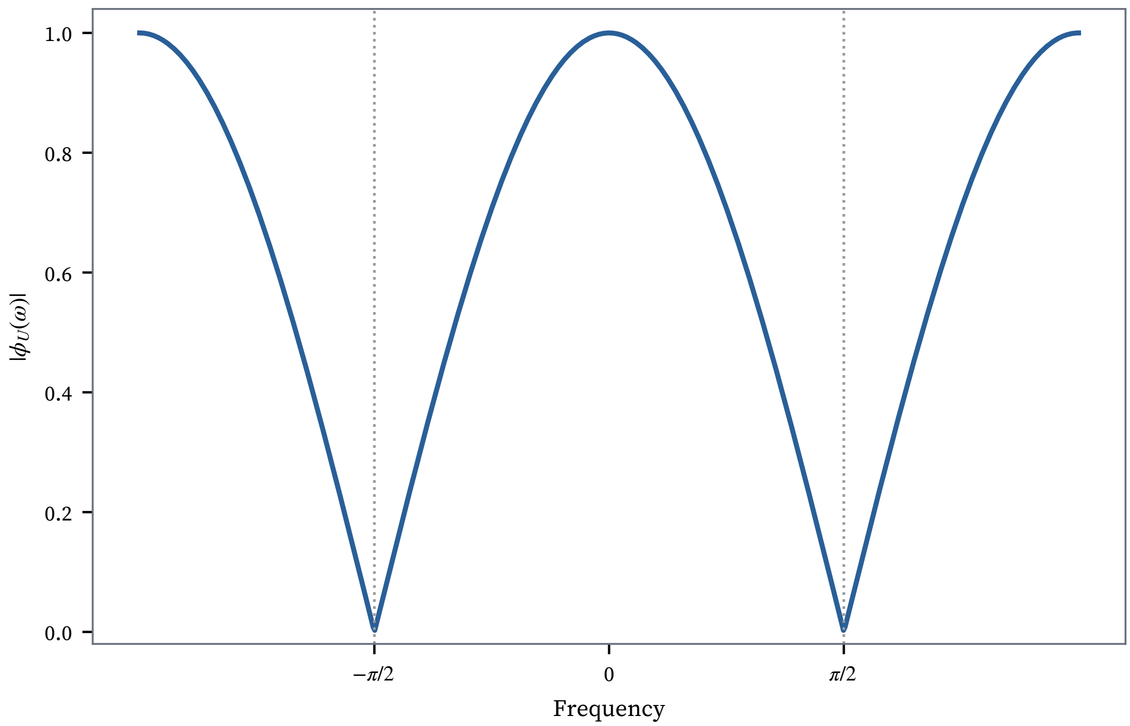

FIGURE A2. Clock multiplier for a two-point timing error

The clock error satisfies $\mathbb{P}(U = 0) = \mathbb{P}(U = 2) = 1/2$, so $\phi_U(\omega) = \{1 + \exp(2i\omega)\}/2$ and $|\phi_U(\omega)| = |\cos(\omega)|$.

so its modulus is $|\cos(\omega)|$. Its zeros occur at $\omega = \pm\pi/2$ on $[-\pi, \pi]$.

Appendix I. European Gas Data and Additional Calculations

I.1. Daily network data and baseline construction

Daily network quantities come from ENTSOG operational records and country-level gas balances come from Eurostat (European Network of Transmission System Operators for Gas 2025; Eurostat 2025). The flow panel is organized at the country–point–direction–day level. When both reporting sides are available for a directed country pair, the country-pair flow uses their average; single-side observations use the available side. Quantities are converted to common daily energy units before aggregation. The analysis keeps route direction, physical point type, and observation dates with each point.

The pre-event service scale uses 2021 observations. Service combines net pipeline entry, LNG, production, and storage withdrawal; storage injection remains a separate quantity. Four component baselines are estimated from 2021 daily data using an intercept, annual sine–cosine terms, and degree-day weather. Predictions enter the denominator B_{it} in (53). The Russian-service allocation and the external, production, and withdrawal adjustments add to the fixed-scale service measure. Market-days with missing aggregate service remain missing in the response path.

I.2. Response profile and temporal resolution

For reporting temporal dispersion, the stored calculation places each weekly mass at its midpoint $h_k = 3 + 7k$. Denote that coarsened variance by $\widehat{V}_W^{N,\mathrm{mid}}$. The daily step profile in (50) adds a within-week variance of four squared days:

$$\widehat{V}_W^N = \widehat{V}_W^{N,\mathrm{mid}} + 4. \tag{A92}$$

The centroid and mass coincide under both resolutions. The variance row reported below uses the weekly-midpoint resolution; the daily-profile point estimate is 29.95 squared days. A loss calculation uses the dispersion at its own delivery resolution. The constant four leaves the delta gradient unchanged. Online Appendix I gives the identity and the corresponding delta calculation.

TABLE A3. Three-week response profile

Event week	Daily response	Cluster-t_{14} 95% interval	Delete-one range
0 (days 0–6)	11.58 pp	[-5.45, 28.61]	[-0.04, 14.49]
1 (days 7–13)	27.43 pp	[10.92, 43.94]	[15.88, 29.32]
2 (days 14–20)	34.62 pp	[11.39, 57.85]	[20.15, 39.96]

Each coefficient is constant within its seven-day bin in (50). Cluster intervals use a Student t critical value with 14 degrees of freedom. Delete-one columns re-estimate the weekly profile after removing one market.

I.3. Network response estimation

The event-study sample covers May 24 through July 4, 2022. Event week −1 is the reference week; weeks −3, −2, 0, 1, 2 interact pre-event Nord Stream exposure with week indicators. Market and calendar-day effects and heating and cooling degree-day controls match the specification in (49). The 21- and 28-day averages use 645 and 855 market-days, respectively, from the same fifteen exposure units.

For window $j \in \{21, 28\}$, let S_{gj} denote market g's score for the zero-coefficient null after partialling out the controls and fixed effects. The exact test enumerates the same 2^{15} sign vectors for both windows and compares each observed statistic to

$$\max_{j\in\{21,28\}} \frac{\left|\sum_g \xi_g S_{gj}\right|}{\left(\sum_g S_{gj}^2\right)^{1/2}}.$$

The resulting familywise p-values are 0.0272 for the 21-day window and 0.0086 for the 28-day window. The marginal exact values, 0.0097 and 0.0086, are retained in the reproduction output.

For the three post-event weekly coefficients, let $b = (\widehat{\beta}_0, \widehat{\beta}_1, \widehat{\beta}_2)^\top$, $h = (3, 10, 17)^\top$, and $s = \mathbf{1}^\top b$. For $M = 7s$, $a = b^\top h/s$, $e_2 = b^\top (h \circ h)/s$, and $V = e_2 - a^2$, the delta gradients are

$$\nabla_b M = 7\mathbf{1}, \qquad \nabla_b a = \frac{h - a\mathbf{1}}{s}, \qquad \nabla_b V = \frac{h \circ h - e_2\mathbf{1} - 2a(h - a\mathbf{1})}{s}. \tag{A93}$$

With the market-clustered covariance matrix $\widehat{\Sigma}_b$, the standard error for the weekly-midpoint functional is $(\nabla q^\top \widehat{\Sigma}_b \nabla q)^{1/2}$, and intervals use the t_{14} critical value. The profile has mass 515.43 percentage-point days, centroid 12.19 days, and weekly-midpoint variance 25.95 days squared. Delete-one estimates give mass 251.95–584.76, centroid 11.71–13.93, and variance 11.97–27.45. For the daily step profile, write a day in bin k as $h_k + J$, where J is uniform on $\{-3, -2, -1, 0, 1, 2, 3\}$. The same within-bin distribution in each bin has mean zero and variance $28/7 = 4$. It follows that the full daily variance is the midpoint variance plus four. This constant leaves the delta gradient unchanged and shifts a variance interval or delete-one range by four squared days. The displayed midpoint statistics are retained at their original resolution.

Alternative service scaling gives 21- and 28-day estimates of 33.2 and 40.0 percentage points with unscaled point data, 26.6 and 28.8 with leave-month-out 2021 scaling, and 17.4 and 19.0 with contemporaneous scaling. The designated specification uses the fixed 2021 scale.

I.4. Physical timing around June 2022

The regulator reference follows the Bundesnetzagentur and Bundeskartellamt Monitoring Report 2022, which records Nord Stream 1 near 60 percent of maximum capacity on June 14 and 40 percent on June 15 (Bundesnetzagentur and Bundeskartellamt 2022). The binary event design uses June 14 as the first reduction date.

For a route flow X_t, let a_t be the median of the preceding fourteen covered daily observations. A screen with drop threshold d and persistence p records a start date t when

$$X_{t+s} \le (1-d)a_t, \qquad s = 0, \ldots, p-1. \tag{A94}$$

The baseline must exceed one percent of the route's positive 2021-day median, and every observation used in the persistence window must be covered. Applying the rule grid to Nord Stream flows within seven days of June 14 gives two distinct starts, June 13 and June 16. These dates produce the physical-origin sensitivity set used in Table 4.

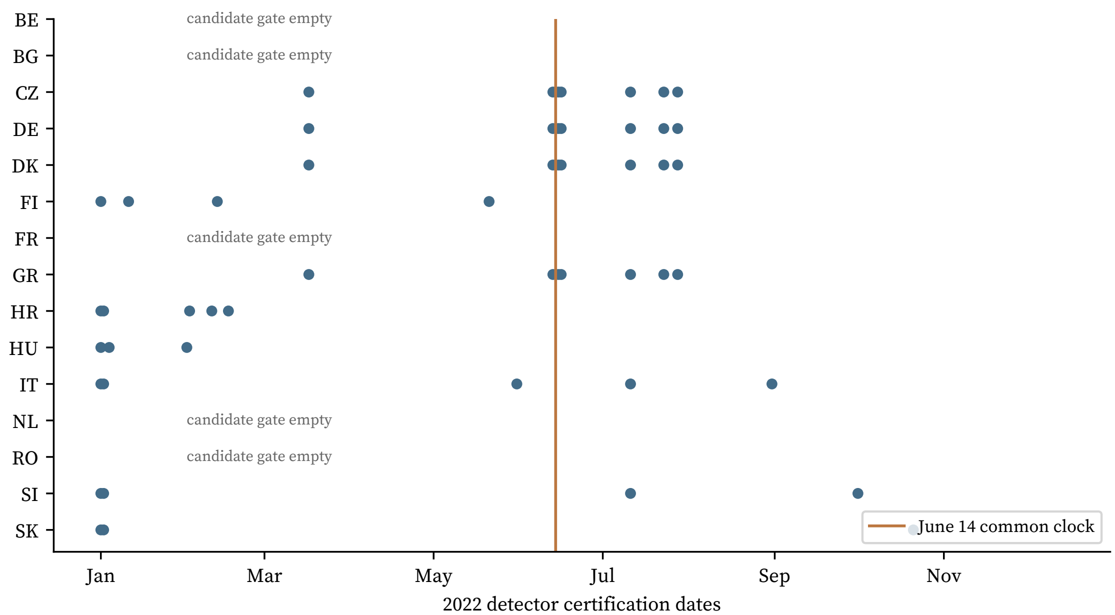

FIGURE A3. Physical timing candidates around recorded origins

The panels report route-flow timing candidates generated by the stated drop-and-persistence rule. The main text uses the June 2022 Nord Stream candidates within the specified neighborhood of the regulator reference.

I.5. Population clock calculation

The population-clock exercise uses Czechia, Germany, Finland, Croatia, Hungary, Italy, and Slovenia, which have complete paths over the target window. Their daily residual-service shares are averaged on the 2022–2024 calendar support and the resulting target is extended by zero outside that support. Let z denote this target. Applying the candidate displacement law to z produces the recorded path $m = A_p z$. The cumulative target is 172.85 share-days.

The disclosure sequence applies the moment equations in (54). Support information yields ranges for the first two latent moments, the clock mean fixes the temporal centroid, and the second clock moment fixes the second latent raw moment. The resulting values are shown below.

This calculation treats the target path and candidate displacement law as fixed inputs to the policy formulas. Sampling uncertainty for the network response and timing uncertainty from the physical candidates enter through their corresponding exercises.

I.6. Documentary operator timing

Operator and supplier records provide civil dates for named physical interruptions. Gasum and Gasgrid document the Imatra shutdown, GRTgaz documents the Germany–France

TABLE A4. Clock information and recovered temporal moments

Timing information	T_0	T_1/T_0	T_2/T_0
Normalization + envelope	172.85	[218.93, 491.93]	[153,132.71, 347,197.59]
+ mean displacement	172.85	398.97	[247,638.58, 263,530.54]
+ second moment	172.85	398.97	256,259.76
Full candidate law	172.85	398.97	256,259.76

The target is the windowed seven-market residual-service path. Temporal location uses days and the normalized second raw moment uses days squared. The first two rows use the empirical displacement support and moment compatibility.

interruption, and Gasgrid documents the Balticconnector shutdown (Gasum 2022; Gasgrid Finland 2022; GRTgaz 2022; Gasgrid Finland 2023). The Gasgrid English-bulletin frame for 2021–2024 contains linked notices for the Imatra shutdown, Balticconnector shutdown, and Balticconnector reopening. Restricting this frame to abrupt shutdowns on retained ENTSOG routes leaves Imatra and Balticconnector.

TABLE A5. Events in the Gasgrid bulletin frame

Event	Linked bulletins	Catalogue decision	Detected offset
Balticconnector shutdown	2	Included	+0 days
Balticconnector reopening	2	Excluded: reopening	—
Imatra shutdown	2	Included	+0 days

Linked notices are consolidated at the event level. Eligibility uses the event type and the presence of the corresponding ENTSOG route. Detected offsets use civil dates.

The reference rule uses an 80-percent drop sustained for three days relative to the preceding fourteen-day median. It matches the documented civil date for both eligible Gasgrid shutdowns and the named Germany–France interruption. Across drop thresholds from 20 to 80 percent, Imatra and Balticconnector also satisfy the 7- and 14-day conditions. The Germany–France interruption resumes before those longer persistence horizons. The complete twelve-rule grid remains in the reproduction output.

Civil-date records correspond to adjacent compatible gas-day labels when the intraday onset is unresolved. The resulting displacement set enters sensitivity analysis as a finite set. Extending the empirical clock law across operators, periods, or disruption classes requires a stated event-selection and transfer model.

Appendix J. Policy Queries and Validation Information

J.1. Proofs for the decision results

The proofs of Proposition 2 and Theorem 2 appear beside their statements in the main paper. The bridge proof and additional constructions follow here.

PROOF OF PROPOSITION 4. The first statement applies the definition of decision identification to the environment fiber. Under (43), adjointness gives $\langle q_a - q_b, \tau\rangle = \langle v_{ab,s}, A_p\tau\rangle = \langle v_{ab,s}, m\rangle$, so every pairwise loss difference is constant on the fiber. If a variable-loss contrast takes opposite signs in two environments, a relative fixed cost chosen between those two contrast values reverses the associated two-action ranking. $\square$

Policy regret compares an action with the action optimal in each admissible state (Manski 2004; Stoye 2009, 2012). Montiel Olea et al. (2026) study sampling-based treatment rules with Gaussian likelihood and partial identification, including the role of randomization. The calculation here conditions on a population moment region and optimizes over deterministic dates and a flexible-provision action. Its formulas translate the clock-information region into that specified decision problem; randomization and sampling risk would define an enlarged problem.

J.2. Execution clocks and decision comparisons

Proposition 2 fixes a nonnegative need profile and quadratic mismatch loss. For $a \in [\underline{a}, \bar{a}]$, the scheduled solution projects $\bar{h}$ onto the interval, with cost $\gamma T_0\{V_\tau + \operatorname{dist}(\bar{h}, [\underline{a}, \bar{a}])^2\}$. The application admits every reported centroid. The loss coefficient and flexible performance are maintained primitives; physical data measure the profile.

Recorded-origin deployment occurs at $G_i + U_i + a$. Reindex $\ell = h - U_i$ and average to obtain (18); absolute cross-moment integrability permits the interchange. Under mean response independence from U_i, optimized recorded-origin and verified-origin losses are $\gamma T_0 V_m$ and $\gamma T_0 V_\tau$. An execution-system upgrade is preferred to continued recorded-origin scheduling when its cost is below their difference, $\gamma T_0 \operatorname{Var}(U)$, provided it enables action at the selected verified-origin date and holds the profile fixed. Learning the law from a validation sample changes the information set used to evaluate this investment. Its value depends on the resulting decision rule and acquisition cost.

Response–clock association matters for the sign of the comparison between fixed-origin rules. Give equal weight to units with $(U_i, \tau_i) = (0, \delta_0)$ and $(2, \delta_2)$. The recorded path is δ_0, with scheduled loss zero; the reference path is $(\delta_0 + \delta_2)/2$, with minimum common-offset loss γ. The common-mean condition in (19) excludes this association. A system that retains recorded-origin execution as an option can continue to use that rule.

The example distinguishes two fixed-origin classes from an enlargement of the feasible action set.

J.3. Observational equivalence and policy choices

Let δ_j denote unit mass at j. For the first-order example take $(p, \tau) = (\delta_0, \delta_1)$ and $(p', \tau') = (\delta_1, \delta_2)$. Both recorded paths equal δ_1; the optimal reference-origin scheduled dates are one and two. The second-order environments and their mode comparison are displayed in Section 3.2. For a fixed cost, compatible environments can also choose the same mode; the comparison is evaluated at that cost.

J.4. Moment regions and deterministic minimax regret

Let $c = M_1/M_0$, $V = V_m$, and let S be the retained finite displacement support with endpoints L and U. Write $\mu = \mathbb{E}[U_i]$ and $w = \mathrm{Var}(U_i)$. The compatible clock moments satisfy

$$L \le \mu \le U, \qquad w_{\min}(\mu) \le w \le (U-\mu)(\mu-L), \qquad \bar{h} = c + \mu, \quad v = V - w \ge 0. \tag{A95}$$

If consecutive support points $s_- \le \mu \le s_+$ bracket the mean, then $w_{\min}(\mu) = (\mu - s_-)(s_+ - \mu)$; at a support point the lower bound is zero. The lower bound follows from the lower convex envelope of u^2 on S, and the upper bound follows from $(u-L)(u-U) \le 0$. Both bounds are attained by two-point laws. Interpolating those laws gives the intervening variances at a fixed mean.

The region imposes moment compatibility and nonnegative response variance. Full recorded-path compatibility can further restrict the admissible clock law and response. Calculated regret on this region therefore bounds regret on the full compatible set. The computations condition on the empirical target, displacement support, and disclosed moments. Sampling uncertainty belongs to the corresponding estimation stage.

A finite check on the relaxation. Take the normalized recorded profile $m = (\delta_{-1} + \delta_1)/2$ and a candidate clock $p = (\delta_0 + \delta_1)/2$. The recorded mean and variance are zero and one. The candidate has mean 1/2 and variance 1/4, so moment correction gives a latent mean of 1/2 and variance 3/4. A nonnegative profile with those moments is $3\delta_0/4 + \delta_2/4$. Yet the candidate clock is incompatible with the full recorded profile for any nonnegative response. Indeed, $m_{-2} = 0$ requires $\tau_{-2} = \tau_{-1} = 0$, and $m_0 = 0$ requires $\tau_0 = \tau_1 = 0$, whereas $m_{-1} = 1/2$ requires $\tau_{-1} + \tau_0 = 1$. This finite example uses the existing averaging equation and shows why the moment region is an outer relaxation. It is an algebraic diagnostic, separate from the empirical clock candidates.

With support information alone, $\bar{h} \in [c+L, c+U]$, $v_- = \max\{0, V - (U-L)^2/4\}$, and $v_+ = V$. With the clock mean disclosed, $\bar{h} = c + \mu$, $v_- = \max\{0, V - (U-\mu)(\mu-L)\}$, and $\nu_+ = V - w_{\min}(\mu)$. Disclosing the variance gives $\nu_- = \nu_+ = V - \mathrm{Var}(U_i)$. Feasible disclosed moments are required. Let $[a_-, a_+]$ denote the corresponding mean range and set $d^2 = (a_+ - a_-)^2/4$.

PROPOSITION A13 (Regret on the moment regions). *For these three regions, the minimax scheduled date is $a^{\mathrm{mm}} = (a_- + a_+)/2$, and the mode-specific worst regrets are*

$$R_S(\lambda) = d^2 + (\nu_+ - \lambda)_+, \qquad R_F(\lambda) = (\lambda - \nu_-)_+, \qquad R^*(\lambda) = \min\{R_S(\lambda), R_F(\lambda)\}. \tag{A96}$$

Flexibility is the minimax choice below the switch, scheduling is the choice above it, and both are minimax at

$$\lambda^* = \begin{cases} (\nu_- + \nu_+ + d^2)/2, & d^2 \le \nu_+ - \nu_-, \\ \nu_- + d^2, & d^2 > \nu_+ - \nu_-. \end{cases} \tag{A97}$$

Moreover, $\sup_{\lambda \ge 0} R^*(\lambda) = \max\{d^2, \lambda^* - \nu_-\}$.

PROOF. At state $(\bar{h}, \nu)$, scheduled regret is $(a - \bar{h})^2 + (\nu - \lambda)_+$, and flexible regret is $(\lambda - \nu)_+$. In the support-only region, the endpoint point-mass clocks attain $\bar{h} = c + L, c + U$ and $\nu = V$, simultaneously maximizing the relevant upper envelopes. Their maximum is minimized at the midpoint. In the other two regions the mean is fixed and the upper variance is attainable. The lower variance gives flexible regret. When $\nu_- = 0$ is active, its feasibility follows by continuously varying an endpoint two-point law in the support-only region, or by interpolating the two extremal laws with the disclosed mean in the fixed-mean region, until clock variance reaches V. Equating the two mode-specific regrets gives (A97). Their piecewise-linear envelope gives the displayed supremum. □

The action set consists of deterministic dates and the flexible mode. Randomized allocation across modes defines a separate decision problem. For $\lambda < \nu_-$ all states prefer flexibility; for $\lambda > \nu_+$ all states prefer the scheduled mode with their respective optimal dates. The interval between these cutoffs records unresolved mode comparisons in the moment relaxation.

J.5. Executed population policy calculations

The seven-market calculation uses the target and candidate displacement law defined in Online Appendix I. The January 2022–December 2024 target is extended by zero. Successive rows disclose summaries of the same law; Figure A4 shows the resulting raw-moment ranges.

All information stages use the same denominator $V_m > 0$. Define $\widetilde{\lambda} = \lambda/V_m$, $\widetilde{\nu} = \nu/V_m$, and $\widetilde{R} = R/V_m$. The normalization preserves every provision-mode comparison. The main table reports $\sup_{\lambda \geq 0} \widetilde{R}$; its 57.35 percent change compares the support-only and mean-informed maxima over the same cost domain. Equation (A96) gives the reduction at each fixed cost. The normalized value of a feasible execution-origin upgrade is $\mathrm{Var}(U)/V_m = 7.71$ percent for this clock construction.

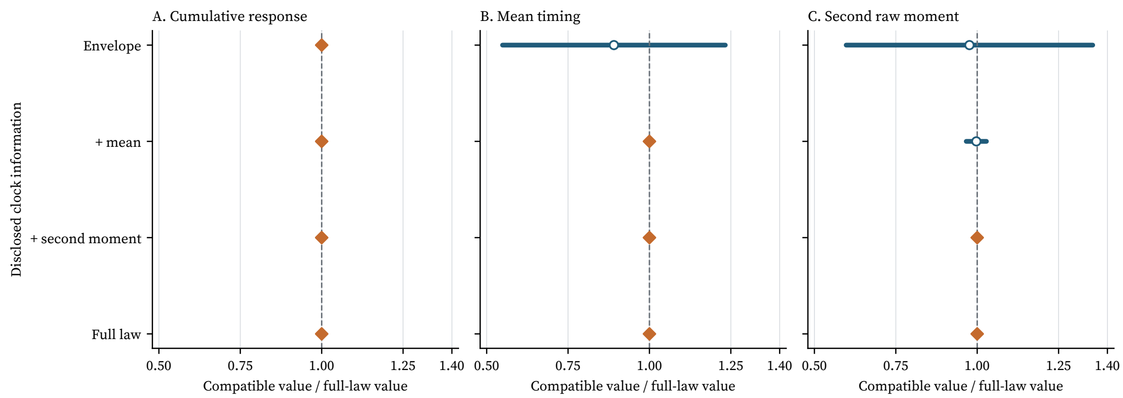

FIGURE A4. Timing information and recovered response queries

The target is an explicitly windowed empirical path. Each panel divides the moment-compatible range by the value under the full candidate law, so the vertical dashed line equals one. A blue segment denotes a remaining compatible interval; an orange diamond denotes point identification. Cumulative response is fixed by normalization. Mean displacement identifies mean timing, and the second displacement moment identifies the second raw moment. The first two outer ranges also condition on the empirical displacement envelope.

TABLE A6. Policy switches over the full cost range

Information	a^{mm}	d^2	λ^*	$\sup_\lambda R^*$
Support	355.4	18,632.2	105,202.3	18,632.2
+ mean	399.0	0.0	96,411.3	7,946.0
+ variance	399.0	0.0	97,086.5	0.0

Dates use days relative to the benchmark origin. Variance, d^2, λ, and regret use squared days per unit response mass after dividing loss by γ. Every nonnegative flexibility cost is covered by (A96)–(A97). The rows use moment-compatible outer regions.

Table A7 evaluates empirical-path equivalence pairs. The first pair changes the scheduled date; the second fixes the date and changes the flexibility threshold. Their full recorded paths agree coordinate by coordinate. These constructions illustrate the information requirements under the common policy loss.

J.6. Storage-option contracts and operational cost units

The second 2022 Stage 1 Strategic Storage-Based Options tender specifies 35,717,500 MWh in 1,099 lots of 32,500 MWh, each with 6,500 MWh callable. Service runs from October

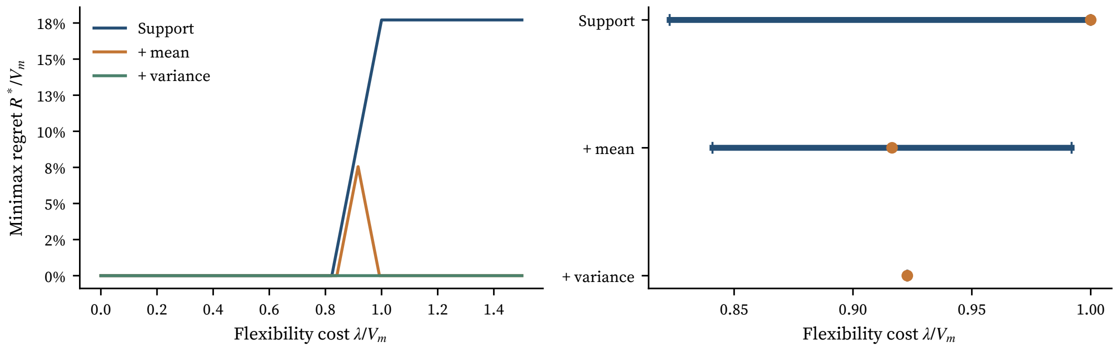

FIGURE A5. Validation information and policy regret

Both panels divide cost by the common V_m. The left panel plots regret as a percentage of V_m. The right panel shows the variance interval governing mode comparisons; orange dots mark deterministic minimax mode switches. The plotting range follows the analytic switches. Table A6 retains the squared-day quantities and all-cost conclusions.

TABLE A7. Policy queries in the empirical-path equivalence constructions

Order	a_A^*	a_B^*	V_A	V_B
1	235.0	508.0	97,086.5	97,086.5
2	310.0	310.0	111,936.5	97,086.5

The rows report moment-order witnesses on the empirical path. A mode disagreement occurs for costs strictly between the two variance entries in the second row. The entire interval is reported. Dates are in days and variances in squared days.

1, 2022 through the January 31, 2023 gas day (Trading Hub Europe 2022a). The official workbook gives 369 awarded rows with per-lot service and capacity prices. Summing each price times awarded lots gives EUR 232,114,035.45 in service fees and EUR 249,130,048.24 in capacity fees (Trading Hub Europe 2022b). Their EUR 481,244,083.69 total agrees with the rounded EUR 481 million announcement (Trading Hub Europe 2022c). Table A8 reports the corresponding unit costs.

TABLE A8. Cost accounting for the second 2022 SSBO tender

Fee component	EUR million	Volume basis	EUR/MWh
Storage service	232.114	Contracted	6.50
Call availability	249.130	Callable	34.88
Combined fees	481.244	Contracted	13.47
Combined fees	481.244	Callable	67.37

Fees sum awarded lots times the corresponding per-lot price in all 369 workbook rows; repeated bid rows remain separate. Contracted volume is 35.7175 TWh; callable volume is 7.1435 TWh. The two combined-fee rows express the same total using different denominators. Commodity charges enter separately on call. Sources: official invitation, award statement, award workbook, and terms dated May 4, 2022.

Section 6 of the terms distinguishes a service fee for the storage commitment, a capacity charge for call availability, and a commodity charge per called MWh linked to the specified gas index plus a contractual surcharge. Section 4 specifies storage and withdrawal obligations; Section 9 requires at least three hours' notice for a call (Trading Hub Europe 2022d). For each contract, delivered quantities q_t, contract-defined index prices P_t, and surcharge z give

$$C_{\text{contract}} = F_{\text{store}} + F_{\text{avail}} + \sum_t (P_t + z) q_t, \qquad \sum_t q_t \leq Q_{\text{callable}}. \tag{A98}$$

The feasible q_t also obeys the service window and storage, withdrawal, and delivery conditions. The workbook identifies both fee components as contracted. The incremental cost relative to a fixed-date alternative additionally uses that alternative's price and obligations. EUR 34.88 per callable MWh measures the contracted availability charge; EUR 67.37 measures the combined fee on the same volume basis.

To connect the timing benchmark to a local operating-cost problem, let $q_h \geq 0$ be a need profile in MWh on a specified contract window, let $Q_0 = \sum_h q_h > 0$, and let $c(d)$ be incremental cost per MWh for a timing displacement d. Suppose c is three times differentiable on the evaluated mismatch range, with $c'(0) = 0$, $c''(0) = 2g > 0$, and $|c'''(d)| \leq M_c$. Taylor's formula gives

$$\begin{aligned} C(a) - C_{\text{match}} &= \sum_h q_h \{c(a-h) - c(0)\} \\ &= g Q_0 \{V_q + (a - \bar{h}_q)^2\} + \mathcal{E}(a), \qquad |\mathcal{E}(a)| \leq \frac{M_c}{6} \sum_h q_h |a-h|^3. \end{aligned} \tag{A99}$$

Here $C_{\text{match}} = \sum_h q_h c(0)$, $\bar{h}_q = \sum_h h q_h / Q_0$, and $V_q = \sum_h q_h (h - \bar{h}_q)^2 / Q_0$. The coefficient g uses EUR per MWh per squared day. A flexible plan that removes timing mismatch at incremental cost K has local threshold $\lambda = K/(gQ_0)$, up to the displayed approximation error. Thus the quadratic benchmark describes a smooth local mismatch technology with a priced curvature and a common need profile. Capacity constraints, lead times, and price-index variation enter the operating problem through their own restrictions.

The executed contract-window profile sets q_h equal to projected German residual service covered by uniform daily call capacity. It contains 6.31 TWh, has centroid 59.79 days from October 1, and has variance 1199.83 squared days. For a fixed-date comparator sharing storage-service and commodity terms, the observed capacity charge gives

$$g^*_{\text{avail}} = \frac{F_{\text{avail}}}{Q_0 V_q} = 34.88 \frac{Q_{\text{callable}}}{Q_0 V_q} = \text{EUR } 0.0329/\text{MWh}/\text{day}^2. \tag{A100}$$

TABLE A9. Contract-window timing-curvature threshold

Quantity	Value
Covered contract-window need	6.314 TWh
Need centroid	59.8 days
Need variance	1,199.8 day^2
Callability price	EUR 249.130 million
Break-even curvature	EUR 0.0329/MWh/day^2
CoDG-equivalent mismatch	58.9 days

The capacity charge prices callability conditional on the storage-service component. The need profile is the projected residual covered by uniform daily call capacity. The final row solves $gd^2 = \text{CoDG}_{DE}$.

The displayed value is the curvature at which best fixed-date scheduling and continuous callability have equal quadratic cost for this profile. It supplies a monetary threshold for g. The seven-market information experiment uses a separate normalized target over three years, so its regret percentages remain on their own scale. Realized draws, commodity prices, the feasible fixed-date procurement technology, and distributional incidence enter a welfare comparison as additional objects.

ENTSOG's 2020 cost-benefit methodology values avoided demand curtailment using the cost of disruption of gas supply and reports Germany at EUR 114.1/MWh in Annex D, Table 7 (European Network of Transmission System Operators for Gas 2020). The contract-window calculation converts the projected German residual from TJ/day to MWh/day and applies a uniform daily call capacity of 58,077.24 MWh across 123 days. The residual is observed on every day; it is positive on 111 days and exceeds daily call capacity on 104. Covered projected shortfall totals 6.314 TWh, so its CoDG value is EUR 720.4 million. The EUR 481.244 million combined fee equals EUR 76.22 per covered MWh, and the gap to the CoDG unit value is EUR 37.88 per covered MWh. This gap is the break-even allowance for commodity call costs and other incremental resource costs under the displayed coverage rule. Realized delivery, system constraints, consumer incidence, and counterfactual procurement costs complete a welfare account.

References

Breunig, Christoph and Jan Johannes, "Adaptive Estimation of Functionals in Nonparametric Instrumental Regression," *Econometric Theory*, 2016, *32* (3), 612–654.

Bundesnetzagentur and Bundeskartellamt, "Monitoring Report 2022: Key Findings and Summary," Technical Report, Bundesnetzagentur and Bundeskartellamt 2022. Published November 2, 2022.

Carrasco, Marine, Jean-Pierre Florens, and Eric Renault, "Linear Inverse Problems in Structural Econometrics: Estimation Based on Spectral Decomposition and Regularization," in

James J. Heckman and Edward E. Leamer, eds., *Handbook of Econometrics*, Vol. 6B, Elsevier, 2007, chapter 77, pp. 5633–5751.

Cocci, Matthew D. and Mikkel Plagborg-Møller, "Standard Errors for Calibrated Parameters," *Review of Economic Studies*, 2025, *92*, 2952–2978.

European Network of Transmission System Operators for Gas, "2nd ENTSOG Methodology for Cost-Benefit Analysis of Gas Infrastructure Projects: Annex D," Technical Report, ENTSOG 2020.

—, "ENTSOG Transparency Platform API: User Manual, Version 3.0," 2025. API documentation.

Eurostat, "Natural Gas Supply Statistics," 2025. Statistics Explained; datasets nrg_cb_gasm and nrg_cb_gas.

Gasgrid Finland, "Gas Supplies through the Imatra Entry Point Have Been Stopped," 2022. 21 May, operational bulletin.

—, "Suspicion of a Leak in the Balticconnector Gas Pipeline between Finland and Estonia," 2023. 8 October, operational bulletin.

Gasum, "Natural Gas Imports from Russia under Gasum's Supply Contract Has Been Halted," 2022. 21 May, supplier statement.

Golub, Gene H. and Victor Pereyra, "The Differentiation of Pseudo-Inverses and Nonlinear Least Squares Problems Whose Variables Separate," *SIAM Journal on Numerical Analysis*, 1973, *10* (2), 413–432.

GRTgaz, "GRTgaz constate un arrêt du flux physique entre la France et l'Allemagne," 2022. Operational statement, June; retained on the successor NaTran website.

Johannes, Jan, Sébastien Van Bellegem, and Anne Vanhems, "Convergence Rates for Ill-Posed Inverse Problems with an Unknown Operator," *Econometric Theory*, 2011, *27* (3), 522–545.

Kaido, Hiroaki, Francesca Molinari, and Jörg Stoye, "Confidence Intervals for Projections of Partially Identified Parameters," *Econometrica*, 2019, *87* (4), 1397–1432.

Kato, Kengo and Yuya Sasaki, "Uniform Confidence Bands in Deconvolution with Unknown Error Distribution," *Journal of Econometrics*, 2018, *207* (1), 129–161.

—, —, and Takuya Ura, "Robust Inference in Deconvolution," *Quantitative Economics*, 2021, *12* (1), 109–142.

Manski, Charles F., "Statistical Treatment Rules for Heterogeneous Populations," *Econometrica*, 2004, *72* (4), 1221–1246.

Molinari, Francesca, "Microeconometrics with Partial Identification," in Steven N. Durlauf, Lars Peter Hansen, James J. Heckman, and Rosa L. Matzkin, eds., *Handbook of Econometrics*, Vol. 7A, Elsevier, 2020, chapter 5, pp. 355–486.

Olea, José Luis Montiel, Chen Qiu, and Jörg Stoye, "Decision Theory for Treatment Choice Problems with Partial Identification," *Review of Economic Studies*, 2026. Advance article rdag015, published February 17.

Santos, Andres, "Instrumental Variable Methods for Recovering Continuous Linear Functionals," *Journal of Econometrics*, 2011, *161* (2), 129–146.

—, "Inference in Nonparametric Instrumental Variables with Partial Identification," *Econometrica*, 2012, *80* (1), 213–275.

Severini, Thomas A. and Gautam Tripathi, "Some Identification Issues in Nonparametric Linear Models with Endogenous Regressors," *Econometric Theory*, 2006, *22* (2), 258–278.

___ **and** ___ , “Efficiency Bounds for Estimating Linear Functionals of Nonparametric Regression Models with Endogenous Regressors,” *Journal of Econometrics*, 2012, *170* (2), 491–498.

Stoye, Jörg, “Minimax Regret Treatment Choice with Finite Samples,” *Journal of Econometrics*, 2009, *151* (1), 70–81.

___ , “Minimax Regret Treatment Choice with Covariates or with Limited Validity of Experiments,” *Journal of Econometrics*, 2012, *166* (1), 138–156.

Tamer, Elie, “Partial Identification in Econometrics,” *Annual Review of Economics*, 2010, *2*, 167–195.

Trading Hub Europe, “Ausschreibung zur Gewährleistung der Versorgungssicherheit: Strategic Storage-Based Options, Stufe 1,” 2022. Second tender, May 30–June 13; service October 1, 2022–February 1, 2023.

___ , “Results SSBO Tender Level 1: Bidding Period 30 May to 13 June 2022,” 2022. Award workbook, Results sheet, cells A1:G370.

___ , “Second SSBO Tender to Increase Security of Supply Completed,” 2022. Press release, June 14.

___ , “Terms and Conditions for the Contracting and Use of Stage 1 Strategic Storage-Based Options,” 2022. English version dated May 4; sections 4, 6, 8, and 9.

Zinde-Walsh, Victoria, “Measurement Error and Deconvolution in Spaces of Generalized Functions,” *Econometric Theory*, 2014, *30* (6), 1207–1246.